

“This document is the Accepted Manuscript version of a Published Work that appeared in final form in *J Am Chem Soc* **2016**, *138* (15), 5093, copyright © American Chemical Society after peer review and technical editing by the publisher. To access the final edited and published work see 10.1021/jacs.6b00972.

## HIERARCHICAL SELF-ASSEMBLY OF POLYOXOMETALATE-BASED HYBRIDS DRIVEN BY METAL COORDINATION AND ELECTROSTATIC INTERACTIONS: FROM DISCRETE SUPRAMOLECULAR SPECIES TO DENSE MONODISPERSE NANOPARTICLES.

Guillaume Izzet,<sup>\* §</sup> Benjamin Abécassis,<sup>†</sup> Dalil Brouri,<sup>‡</sup> Madeleine Piot,<sup>§</sup> Benjamin Matt,<sup>§</sup> Stefano Artin Serapian,<sup>£</sup> Carles Bo<sup>£,§</sup> and Anna Proust<sup>§</sup>

<sup>§</sup> Sorbonne Universités, UPMC Univ. Paris 06, CNRS UMR 8232, Institut Parisien de Chimie Moléculaire, Université Pierre et Marie Curie, 4 place Jussieu, F-75005 Paris, France.

<sup>†</sup> Laboratoire de Physique des Solides, Univ. Paris-Sud, CNRS UMR 8502, 91405 Orsay Cedex, France.

<sup>‡</sup> Sorbonne Universités, UPMC Univ. Paris 06, CNRS UMR 7197, Laboratoire de Réactivité de Surface, Université Pierre et Marie Curie, 4 place Jussieu, F-75005 Paris, France.

<sup>£</sup> Catalan Institute of Chemical Research (ICIQ), The Barcelona Institute of Science and Technology, Av. dels Països Catalans 16, 43007 Tarragona, Spain.

<sup>§</sup> Departament de Química Física i Inorgànica, Universitat Rovira i Virgili, Av. dels Països Catalans, 26, 43007 Tarragona, Spain.

*Supporting Information Placeholder*

---

**ABSTRACT:** The metal-driven self-assembly processes of a covalent polyoxometalate (POM)-based hybrid bearing remote terpyridine binding sites have been investigated. In a strongly dissociating solvent, a discrete metallomacrocyclic, described as a molecular triangle, is formed and characterized by 2D diffusion NMR spectroscopy (DOSY), small-angle X-ray scattering (SAXS) and molecular modeling. In a less dissociating solvent, the primary supramolecular structure, combining negatively charged POMs and cationic metal linkers, further self-assembles through intermolecular electrostatic interactions in a reversible process. The resulting hierarchical assemblies are dense monodisperse nanoparticles composed of *ca.* 50 POMs that were characterized by SAXS and High-Resolution Transmission Electron Microscopy (HR-TEM). This multi-scale organized system directed by metal coordination and electrostatic interactions constitutes a promising step for the future design of POM self-assemblies with controllable structure-directing factors.

---

## INTRODUCTION

The control of molecular organization from small molecular building blocks by self-assembly is a major challenge in supramolecular chemistry.<sup>1</sup> The design of nanoscale materials with hierarchical order and complexity opens up important perspectives for a wide range of technological applications.<sup>2-5</sup> In this context, the elaboration of functional materials integrating polyoxometalates (POMs) as molecular building blocks is particularly attractive owing to their various properties and potential applications.<sup>6-8</sup> POMs are anionic nanosized molecular metal-oxides that bridge the gap between small oxo-metal complexes and bulk metal-oxides. Nanostructured assemblies containing POMs have been mostly developed from POM-based surfactant hybrids.<sup>9,10</sup> In such systems, the POM is associated with amphiphilic moieties either through electrostatic interaction or by a covalent anchorage. The formation of highly ordered films,<sup>11</sup> liquid crystals phases,<sup>12-14</sup> hollow spheres,<sup>15-17</sup> micelles,<sup>18</sup> micro-emulsion<sup>19</sup> or smart photo-responsive systems<sup>20</sup> through self-assembly processes of POMs has thus been described. Metal-directed self-assembly is also a powerful tool

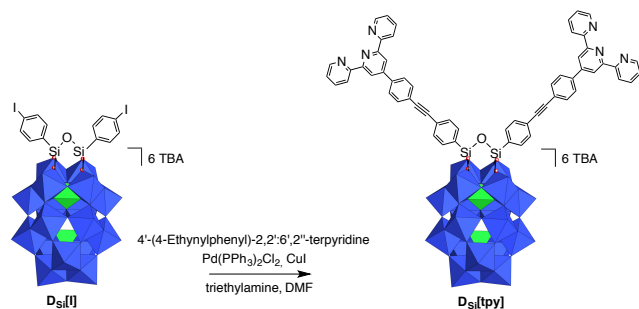
for the synthesis of discrete 0D to extended 3D assemblies.<sup>21,22</sup> As regards POM chemistry, a plethora of POM-based coordination polymers have been obtained through reactions of POMs with organic ligands and metal salts, most often under hydrothermal conditions.<sup>23,24</sup> While this method has proven successful in the production of crystalline open-framework materials with 3D topologies, it does not afford much control of dimensionality. In contrast, metal driven self-assembly of preformed covalent POM hybrids bearing remote binding sites has been very scarcely described in the literature, while this approach is well-suited for the rational design of organized nano-architectures.<sup>25-29</sup>

Relying on our expertise in the field of covalent POM-based hybrids, this drove us to elaborate controllable POM-based nano-architectures through metal directed self-assembly. We recently described a covalent POM-based molecular triangle and characterized it through a combination of complementary analytical techniques (DOSY NMR, SAXS and TWIM MS) that proved to be relevant tools for probing the chemical structure of such large assemblies.<sup>30</sup> The system developed was obtained through the reaction between an organosilyl functionalized Dawson-type POM displaying two terminated-pyridine binding sites and one equivalent of a linear neutral metal linker, *i.e.* *trans*-[PdCl<sub>2</sub>(CH<sub>3</sub>CN)<sub>2</sub>]. We herein explore the metal driven self-assembly of the bis-terpyridine analogue, in the presence of a cationic metal linker. In such a system, the combination of negatively charged POMs and cationic metal linkers favour the aggregation of the primary self-assembled structures into larger multi-scale assemblies through intermolecular electrostatic interactions.<sup>31-35</sup> We also report that the aggregation of the primary supramolecular structures is controlled by the nature of the solvent.

## RESULTS AND DISCUSSION

### Synthesis of the POM-based molecular platform

The POM-based building block [P<sub>2</sub>W<sub>17</sub>O<sub>61</sub>{O(Si-C<sub>29</sub>H<sub>18</sub>N<sub>3</sub>)<sub>2</sub>}]<sup>6-</sup> denoted **D<sub>Si</sub>[tpy]**<sup>36</sup> contains two terpyridine (tpy) units connected to the mono-lacunary site of a Dawson-type α<sub>2</sub>-[P<sub>2</sub>W<sub>17</sub>O<sub>61</sub>]<sup>10-</sup> through a Si–O–Si anchorage. Its synthesis is performed in one step from the iodo-aryl terminated POM-based platform **D<sub>Si</sub>[I]** by adapting to our previously reported procedure involving a Sonogashira cross-coupling reaction (scheme 1).<sup>37</sup> The hybrid **D<sub>Si</sub>[tpy]** is isolated as a tetrabutyl ammonium (TBA) salt in good yield and characterized by <sup>1</sup>H and <sup>31</sup>P NMR spectroscopies, mass spectrometry, elemental analyses and FT-IR spectroscopy (see SI).



**Scheme 1.** Synthetic route to the **D<sub>Si</sub>[tpy]** hybrid. In the polyhedral representation, the WO<sub>6</sub> octahedra are depicted with oxygen atoms at the vertices and metal cations buried inside. Color code: WO<sub>6</sub> octahedra, blue; PO<sub>4</sub> tetrahedra, green.

### Formation of a discrete molecular triangle

Terpyridine ligands produce a linear arrangement when coordinated to an octahedral metal centre such as Fe<sup>II</sup>. The addition of [Fe(H<sub>2</sub>O)<sub>6</sub>](ClO<sub>4</sub>)<sub>2</sub> to a colorless solution of **D<sub>Si</sub>[tpy]** (1 mM) in DMSO instantly produces the characteristic purple colour of the low spin Fe(II) bis-terpyridine complexes. <sup>1</sup>H NMR monitoring of the progressive addition of [Fe(H<sub>2</sub>O)<sub>6</sub>](ClO<sub>4</sub>)<sub>2</sub> to a solution of **D<sub>Si</sub>[tpy]** (1 mM in DMSO-*d*<sub>6</sub>) shows the progressive formation of a new species displaying the same number of signals in the aromatic region and the concomitant disappearance of **D<sub>Si</sub>[tpy]**. The reaction is total after the addition of 1 equiv. of Fe per POM, in agreement with the formation of a supramolecular species displaying a 1:1 stoichiometry between the POM and the metal linker.

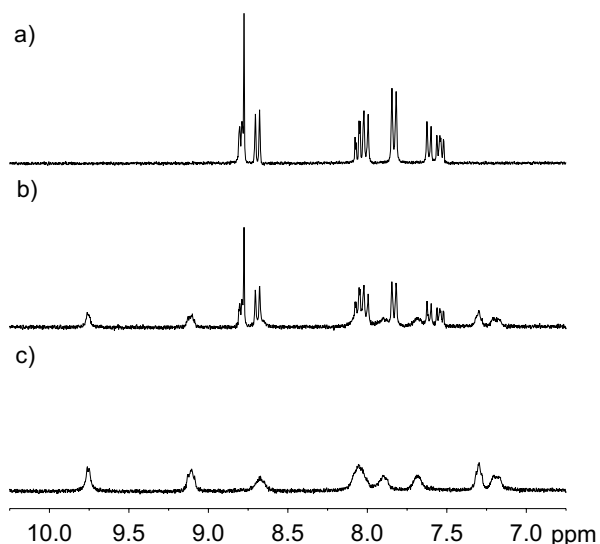


**Figure 1.**  $^1\text{H}$  NMR (300 MHz, aromatic region) monitoring of the progressive addition of  $[\text{Fe}(\text{H}_2\text{O})_6](\text{ClO}_4)_2$  to a 1 mM solution of  $\text{DSi}[\text{tpy}]$  in  $\text{DMSO}-d_6$ . a) before addition, b) 0.5 eq., c) 1.0 eq.

The  $^1\text{H}$  NMR signals of the resulting supramolecular species are significantly broader than that of the parent hybrid  $\text{DSi}[\text{tpy}]$ . This is interpreted as the formation of larger species since the NMR signal line width is determined by  $T_2$  relaxation, which is attenuated in large structures. The addition of an excess of diethyl ether to a solution containing  $\text{DSi}[\text{tpy}]$  and one equiv. of  $[\text{Fe}(\text{H}_2\text{O})_6](\text{ClO}_4)_2$  in DMSO leads to the precipitation of a purple solid. The infrared spectrum of the solid shows the absence of perchlorate while the relative intensity of the signal corresponding the TBA cations are slightly attenuated (Figure S2). This suggests that upon the precipitation of the solid, the perchlorate ions remain in solution as tetrabutylammonium salt. Finally, upon dissolution of the purple solid in  $\text{DMSO}-d_6$ ,  $^1\text{H}$  NMR signals of the resulting solution in the aromatic region match those of the solution prior to precipitation, suggesting that perchlorate ions are not associated to the metallomacrocycle (Figure S3).

Diffusion-ordered NMR spectroscopy (DOSY) gives access to the translational diffusion coefficient, which is related to the size of the molecular assembly.<sup>38,39</sup> DOSY NMR experiments were performed on a 1 mM solution of  $\text{DSi}[\text{tpy}]$  in  $\text{DMSO}-d_6$  before and after the addition of 1 equiv. of  $[\text{Fe}(\text{H}_2\text{O})_6](\text{ClO}_4)_2$  at  $T = 300$  K. All aromatic signals of the resulting supramolecular assembly give a unique diffusion coefficient, significantly lower than that of the parent hybrid (Figures S4 and S5,  $D(\text{DSi}[\text{tpy}]) = 8.0 \times 10^{-11} \text{ m}^2 \cdot \text{s}^{-1}$ ,  $D([\text{DSi}[\text{tpy}]\cdot\text{Fe}] = 2.9 \times 10^{-11} \text{ m}^2 \cdot \text{s}^{-1}$ ). This suggests that all aromatic signals arise from species of similar shape and size, which precludes the formation of linear oligomeric species. The calculated hydrodynamic radius of a spherical particle with  $D = 2.9 \times 10^{-11} \text{ m}^2 \cdot \text{s}^{-1}$  (considering  $T = 300$  K and  $\eta = 2.18 \text{ mPa} \cdot \text{s}$ <sup>40</sup>) is  $r_H = 3.5$  nm according to the Stokes-Einstein equation. In the previously reported system based on a bis-pyridine analogue, the metal driven self-assembly led to a molecular triangle that was unambiguously characterized.<sup>30</sup> Owing to the structural similarity between both POM building blocks, it is likely that the supramolecular assemblies here characterized by DOSY NMR consist of molecular triangles.

To gain further insight into the structure of the cyclic oligomer, we seek to obtain the optimized structure of the molecular triangle, using density functional theory DFT as implemented by the program *ADF* (see SI for more details).<sup>41,42</sup> Its sheer size, characterized by 6804 electrons, constitutes a considerable computational challenge: it was therefore decided to start tackling the problem by breaking the system down into better-manageable fragments. We thus begin by performing separate preliminary optimizations of smaller species: a free unit of  $\text{DSi}[\text{tpy}]$  as depicted in Scheme 1; and a “naked” (Dawson-free) triangle with neutral  $[\text{H}_2\text{C}-\text{O}-\text{CH}_2]$  vertices replacing the formal  $[\text{O}_2\text{Si}-\text{O}-\text{SiO}_2]^4$ , and  $\text{Zn}^{2+}$  replacing  $\text{Fe}^{2+}$ . Both of these initial optimizations are performed using the BP86 density functional, featuring the exchange functional developed by Becke,<sup>43</sup> in conjunction with the P86 correlation functional developed by Perdew,<sup>44,45</sup> we also apply the D3 dispersion correction by Grimme<sup>46</sup> in combination with Becke-Johnson damping (D3(BJ)).<sup>47,48</sup> Electrons on all elements are modeled using a triple- $\zeta$  Slater-type basis set with one polarization function (TZP); core electrons are kept frozen, and treated with an appropriate relativistic frozen-core potential. Relativistic effects are introduced by means of the *zeroth-order regular approximation* (ZORA) in its scalar-relativistic form.<sup>49,50</sup> Electron integrals are numerically evaluated using Becke’s integration grid<sup>51</sup> (quality: good).<sup>52</sup> Furthermore, at each step of the optimization, self-consistent field equations are solved using the non-standard *indirect linear-expansion shooting technique* (LISTI).<sup>53</sup> this choice is found to be extremely useful in overcoming convergence issues. In order to better reflect

experimental conditions, effects of DMSO are implicitly accounted for using the *conductor-like screening model for real solvents* (COSMO-RS) by Klamt *et al.*,<sup>54-57</sup> evaluation of the solvent cavity is performed by using the set of elemental radii purposely developed in 1998.<sup>57</sup> Finally, we note that the naked triangle is treated, with the  $D_3$  symmetry point group. Next, full molecular triangles are constructed by removing the  $[\text{H}_2\text{C}-\text{O}-\text{CH}_2]$  vertices from the optimized “naked” structure, and replacing each of them with the  $[\text{P}_2\text{W}_{17}\text{O}_{61}(\text{OSi}_2)]^{6-}$  part of the optimized  $\mathbf{D}_{\text{Si}}[\text{tpy}]$  (*i.e.* omitting tpy units beyond the  $\text{Si}-\text{C}_{\text{Ar}}$  bond); Si–O–Si units are roughly positioned on the former coordinates of C–O–C vertices. The orientation of Dawson anions with respect to the plane of the molecular triangle gives rise to two possible isomers. With the aid of single-point energy calculations, conducted at the same level of theory described in the previous paragraph, we find that the lowest-energy isomer of the triangle is the one in which one of the POMs is angled away from the plane in the opposite direction compared to the other two (Figure 2), as found for the previously reported bis-pyridine polyoxometalate-based molecular triangle.<sup>30</sup> We finally proceed to optimize the lowest-energy isomer of the triangle using a special two-level treatment. For the Dawson anions; Si–O–Si units and adjacent phenyl rings;  $\text{Zn}^{2+}$  cations; and chelating N atoms in the tpy unit; we apply the same treatment used in the preliminary optimizations and single-point calculations. On the other hand, remaining regions are conveniently treated at a lower level of theory, which crucially allows to reduce computational time: the TZP basis set is thus replaced by a double- $\zeta$  counterpart, with no polarization functions (DZ); in addition, a coarser version of Becke’s grid is used for evaluating electronic integrals (quality: normal).<sup>51,52</sup> Co-ordinates of the optimized molecular triangle are provided in Table S1 and are also available on-line.<sup>58</sup> The tendency of each Si unit to preserve its tetrahedral structure, with O–Si–O angles of  $\sim 109^\circ$ , combined with the fact that the  $[\text{O}_4]$  lacunae in Dawson anions cannot be distorted from their rectangular shape, lead to a certain amount of strain in the supramolecular structure: this translates into the organic moieties adopting a slight curvature, at the expense of some loss in aromaticity, and the Dawson moieties ending up slightly closer than expected. Such distortion is indeed confirmed by alternatively optimizing the triangle with the hybrid method *ONIOM*,<sup>59</sup> as implemented by the *Gaussian09* software package:<sup>60</sup> further details for this accessory optimization are given as SI, and co-ordinates are reported in Table S2 and are available on-line.<sup>58</sup>

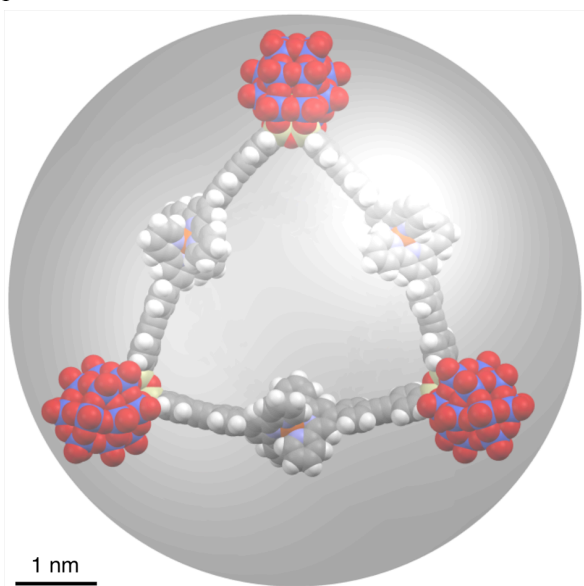


**Figure 2.** Comparison of the energy-minimized structure of the molecular triangle  $\text{Zn}^{2+}$ -analogue  $[(\mathbf{D}_{\text{Si}}[\text{tpy}])_3.\text{Zn}_3]$  with a 3.5 nm radius sphere.

On the other hand, we note that in the optimized  $\mathbf{D}_{\text{Si}}[\text{tpy}]$  alone, where the organic tpy units are ‘open’ and there is no source of strain, organic linkers remain straight. The energy-optimized structure of the molecular triangle has a radius of *ca.* 3.3 nm that is close to the calculated hydrodynamic radius  $r_{\text{H}} = 3.5$  nm deduced from DOSY experiments. The modelisation of a molecular triangle by a sphere particle is very simplistic since it does not account for its anisotropic and hollow shape and it neither considers the contribution of the solvent and the TBA to the translation diffusion of the overall assembly. However, as for the previous supramolecular triangle,<sup>30</sup> this model is fairly consistent with the computational optimized structure.

In order to complete the characterization of the cyclic supramolecular assembly, we performed SAXS (Small-Angle X-ray Scattering) experiments on dispersion of  $\mathbf{D}_{\text{Si}}[\text{tpy}]$  in  $\text{DMSO}-d_6$  before and after the addition of 1 equiv. of  $[\text{Fe}(\text{H}_2\text{O})_6](\text{ClO}_4)_2$ . SAXS is known to give insightful structural information on objects with sizes ranging from 1 to 100 nm.<sup>61,62</sup> We and others have successfully used SAXS to characterize POM-based supramolecular assemblies.<sup>30,63-65</sup>

Figure 3a shows the SAXS pattern for the solvent, a solution of the molecular building-block **D<sub>Si</sub>[tpy]** (1 mM in DMSO-*d*<sub>6</sub>) and the resulting cyclic assembly. These SAXS patterns are very similar to those obtained in the previous bis-pyridine POM-based system. While the solvent pattern is almost flat, a significant SAXS signal is visible for the molecular building-block **D<sub>Si</sub>[tpy]**, consistent with well-dispersed nanometric objects. The small decrease in intensity at small wave vectors is caused by strong electrostatic interactions between these highly charged objects. The SAXS diagram of **D<sub>Si</sub>[tpy]** (1 mM in DMSO-*d*<sub>6</sub>) in the presence of 1 equiv. of [Fe(H<sub>2</sub>O)<sub>6</sub>](ClO<sub>4</sub>)<sub>2</sub> displays additional oscillations that correspond to distance larger than the POMs dimension. The theoretical SAXS pattern of the energy-minimized structures of the molecular triangle [**(D<sub>Si</sub>[tpy])<sub>3</sub>.Fe<sub>3</sub>**] (in which Zn have been replaced by Fe atoms) have been computed using the program CRY SOL (Figure 3b)<sup>66</sup> without any adjustment of free parameters. If we ignore the decrease in intensity caused by the electrostatic interactions, we notice that the intensity at small *q* values (*ca.* 0.03 Å<sup>-1</sup>), which is proportional to the molar mass of the molecular system in case of monodisperse assemblies<sup>67</sup> is perfectly reproduced, which supports the triangular structure. A slight difference is however observed in the first oscillation, suggesting that the POM-POM distance in the calculated molecular triangle is underestimated possibly due to the bent shape of the organic linker. This also may suggest the formation of larger cyclic oligomeric species such as a molecular square. To this end, the structure of a potential molecular square was also investigated by DFT calculations, using the same methodology as previously described for the molecular triangle. The co-ordinates of the resulting optimized structure (featuring pairs of POMs on opposite vertices oriented in the same direction) are given in Table S3 and published on-line.<sup>58</sup> When computing the SAXS patterns of the energy-minimized structure of the molecular square [**(D<sub>Si</sub>[tpy])<sub>4</sub>.Fe<sub>4</sub>**] (Figure S6), the first oscillation is better reproduced than for the molecular triangle [**(D<sub>Si</sub>[tpy])<sub>3</sub>.Fe<sub>3</sub>**]. However, the calculated intensity either at small wave vectors (*ca.* 0.03 Å<sup>-1</sup>) and large wave vectors (*ca.* 0.4-0.6 Å<sup>-1</sup>) does not satisfactory fit with the experimental data, so that the molecular square was not further considered.

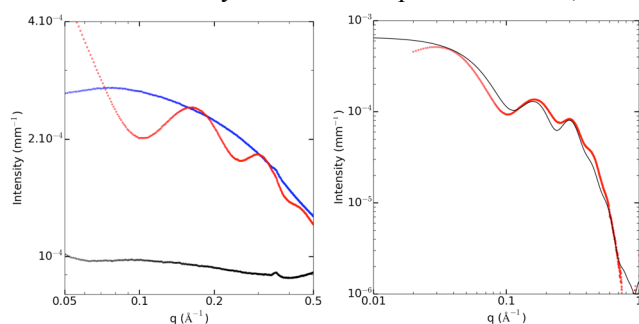


**Figure 3.** Left) SAXS pattern of the solvent (DMSO-*d*<sub>6</sub>, black), a solution of the molecular building-block **D<sub>Si</sub>[tpy]** (1 mM in DMSO-*d*<sub>6</sub>, blue) and the resulting molecular triangle [**(D<sub>Si</sub>[tpy])<sub>3</sub>.Fe<sub>3</sub>**] (red) Right) Comparison of the experimental SAXS pattern of [**(D<sub>Si</sub>[tpy])<sub>3</sub>.Fe<sub>3</sub>**] (red) to the theoretical SAXS intensity (computed using CRY SOL) of the optimized structure (black).

### Aggregation of the supramolecular triangles

Upon the addition of any polar solvent (CD<sub>3</sub>CN, acetone-*d*<sub>6</sub>, D<sub>2</sub>O...) to a solution of [**(D<sub>Si</sub>[tpy])<sub>3</sub>.Fe<sub>3</sub>**] in DMSO-*d*<sub>6</sub>, ill-defined <sup>1</sup>H signals appears in the aromatic region while the solution remains homogeneous and displays its characteristic purple coloration attesting the persistence of the Fe(II) bis-terpyridine complexes. NMR DOSY experiments in such solvent mixtures failed to obtain <sup>1</sup>H signals in the aromatic region. This is characteristic of colloidal systems displaying low T<sub>2</sub> relaxation.<sup>68</sup> The <sup>1</sup>H NMR spectrum of a solution of **D<sub>Si</sub>[tpy]** (1 mM) in the presence of 1 equiv. of [Fe(H<sub>2</sub>O)<sub>6</sub>](ClO<sub>4</sub>)<sub>2</sub> in a mixture of DMSO-*d*<sub>6</sub>/CD<sub>3</sub>CN (1:1, v/v) shows both signals of the discrete molecular triangle [**(D<sub>Si</sub>[tpy])<sub>3</sub>.Fe<sub>3</sub>**] and those ill-defined of the new supramolecular assemblies. However in a DMSO-*d*<sub>6</sub>/CD<sub>3</sub>CN (1:4, v/v) mixture only <sup>1</sup>H NMR signals of the new species are observed (Figure 4a). Interestingly, upon removal of CD<sub>3</sub>CN from DMSO-*d*<sub>6</sub>/CD<sub>3</sub>CN mixtures containing **D<sub>Si</sub>[tpy]** in the presence of 1 equiv. of [Fe(H<sub>2</sub>O)<sub>6</sub>](ClO<sub>4</sub>)<sub>2</sub>, the <sup>1</sup>H NMR signals of the molecular triangle [**(D<sub>Si</sub>[tpy])<sub>3</sub>.Fe<sub>3</sub>**] are quantitatively restored, attesting the reversibility of the process.

SAXS experiments were performed with the same DMSO-*d*<sub>6</sub>/CD<sub>3</sub>CN mixtures containing **D<sub>Si</sub>[tpy]** (1 mM) and 1 equiv. of [Fe(H<sub>2</sub>O)<sub>6</sub>](ClO<sub>4</sub>)<sub>2</sub>. The signal intensity in the low-*q* region significantly increases with the molar fraction of CD<sub>3</sub>CN suggesting the formation of aggregated species. The signal intensity in the low-*q* region (*ca.* 0.03 Å<sup>-1</sup>) is enhanced by a factor of *ca.* 6 and *ca.* 18 in DMSO-*d*<sub>6</sub>/CD<sub>3</sub>CN (1:1, v/v) and (1:4, v/v) mixtures respectively (Figure 4b). Hence, a 18 fold increase between the molecular triangle in DMSO-*d*<sub>6</sub> signal and that of the assembly in a DMSO-*d*<sub>6</sub>/CD<sub>3</sub>CN (1:4, v/v) mixture is consistent with an aggregate composed of *ca.* 54 POMs. From the Guinier regime of SAXS curve<sup>69</sup> in the DMSO-*d*<sub>6</sub>/CD<sub>3</sub>CN (1:4, v/v) mixture, we can also extract a radius of gyration of the aggregates *r<sub>g</sub>* = 3.9 nm. Interestingly the oscillations at *q* > 10<sup>-1</sup> nm<sup>-1</sup> characteristic of the molecular triangle [**(D<sub>Si</sub>[tpy])<sub>3</sub>.Fe<sub>3</sub>**], albeit attenuated, are still present in the SAXS patterns in all DMSO-*d*<sub>6</sub>/CD<sub>3</sub>CN mixtures. This indicates that the new su-



pramolecular assembly is formed by the aggregation of the molecular triangle and remains nanostructured, the molecular triangle acting as a secondary building unit of the overall supramolecular assembly. We previously described the crystal structure of a silyl-pyrene terminated derivative of a Dawson-type POM as a tetrabutyl ammonium salt.<sup>70</sup> In the crystal packing, the volume occupied by a POM-based hybrid is  $4520 \text{ \AA}^3$ . A sphere with  $r = 3.9 \text{ nm}$ , would thus contain *ca.* 55 POMs that is amazingly very close to the 54 POMs per assembly obtained by SAXS. This suggests that the nanoparticle-like assemblies have a maximum compactness.

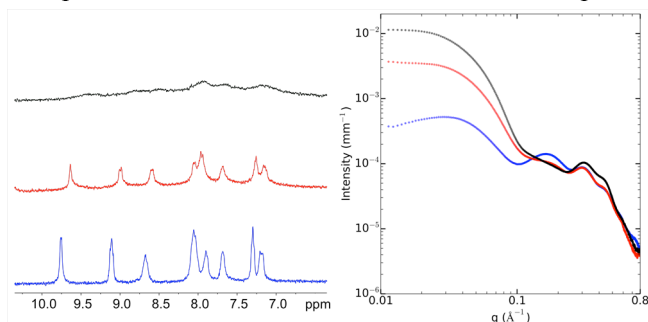


**Figure 4.** <sup>1</sup>H NMR spectra (300 MHz, left) and SAXS curves (right) of solutions of **D<sub>Si</sub>[tpy]** (1 mM) in the presence of 1 equiv. of **[Fe(H<sub>2</sub>O)<sub>6</sub>](ClO<sub>4</sub>)<sub>2</sub>** in DMSO-*d*<sub>6</sub> (blue), DMSO-*d*<sub>6</sub>/CD<sub>3</sub>CN (1/1) (red) and DMSO-*d*<sub>6</sub>/CD<sub>3</sub>CN (1/4) (black).

In the previous bis-pyridine POM-based supramolecular triangle, the binding sites were coordinated to a neutral metal linker, *i.e.* Pd<sup>II</sup>Cl<sub>2</sub>. This system did not self-assemble into a more complex species when changing the composition of the solvent. In the present case, the discrete cyclic coordination oligomer **[(D<sub>Si</sub>[tpy])<sub>3</sub>·Fe<sub>3</sub>]** presents a regular alternation of anionic (POMs) and cationic (metal) moieties, which is likely to favor aggregation through electrostatic interactions. The aggregation processes are dictated by the nature of the solvent and particularly its dissociating ability. In a strongly dissociating solvent such as DMSO, the electrostatic interaction between the cyclic oligomers is weak so that the discrete molecular triangles are observed. In contrast, in a lower dissociating solvent such as acetonitrile, the metal-macrocycles act as secondary building units and further self-assemble in small dense nanoparticles whose anionic nature provide stability in solution.<sup>33</sup>

High-Resolution Transmission Electron Microscopy (HR-TEM) of the dispersed supramolecular assembly was performed after the deposition of few drops of a solution of **D<sub>Si</sub>[tpy]** (25 μM) in the presence of 1 equiv. of **[Fe(H<sub>2</sub>O)<sub>6</sub>](ClO<sub>4</sub>)<sub>2</sub>** in acetonitrile on a Cu grid covered with an amorphous carbon film. Electron micrographs unambiguously show the presence of monodisperse small nanoparticle-like assemblies with  $7.5 \pm 1 \text{ nm}$  diameters (Figure 5), in full agreement with the radius of gyration obtained by SAXS. Inspection of the particles allows the observation of nanometer size POMs that appear more contrasted than the covalent organic tether and the TBA counter-ions due to their important electron density.

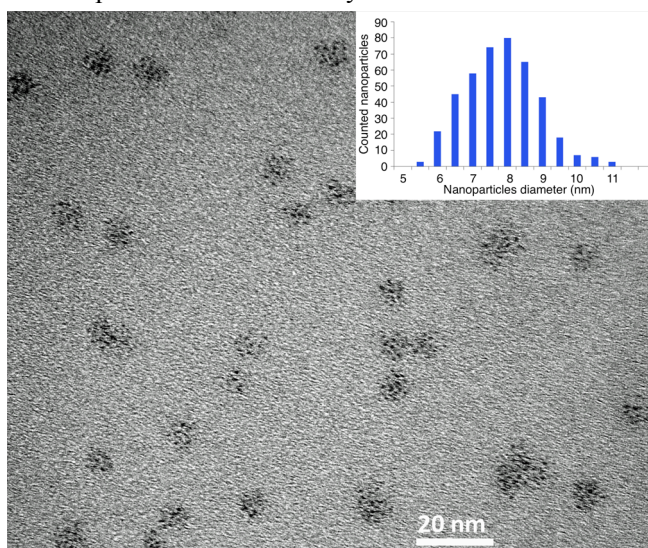
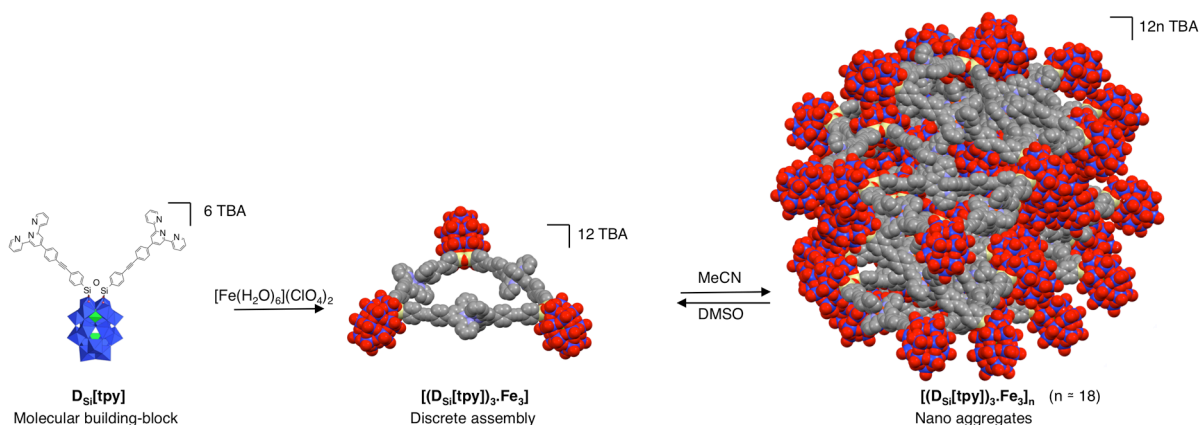


**Figure 5.** HR-TEM micrographs and size histogram (inset) of the nanoparticle-like assemblies **[(D<sub>Si</sub>[tpy])<sub>3</sub>·Fe<sub>3</sub>]<sub>n</sub>**.

The chemical analysis by EDS shows the presence of the main elements constituting the particles (i.e. W, O, C, Si and Fe, Figure S7). No Cl atom is present in the particle, in agreement with the absence of perchlorate anion. In contrast electron micrographs of dispersed **D<sub>Si</sub>[tpy]** in acetonitrile do not show any organization of the POMs(Figure S8).

Important number of self-assemblies of POMs lead to the formation of large hollow structures such as vesicles or blackberry-like structures (usually in the 30-100 nm scale).<sup>10</sup> Similarly POM-based paddle-wheel macroclusters<sup>31</sup> formed by metal-directed self-assembly of a hexamolybdate functionalized with a carboxylic acid unit coordinated to copper ions also assemble into such large hollow-like structure in suitable solvents. We herein report a second type of a hierarchical organization from POM-based building blocks to discrete supramolecular assemblies and then to larger nanoscales structures. In the present case the POM-based supramolecular triangles self-assemble into unprecedented dense monodisperse nanoparticles. The difference between these two types of assemblies probably arises from the presence of the electrostatic interactions between the primary supramolecular assemblies due to the presence of negatively charged POMs and cationic metal linkers within their structure.



**Scheme 2.** Schematic representation of the formation of the nanosized aggregates by hierarchical self-assembly of **D<sub>Si</sub>[tpy]** upon complexation with Fe<sup>2+</sup>.

While the size of the reported blackberry structures vary according to the composition of the solvent, in our system <sup>1</sup>H NMR shows that in DMSO-*d*<sub>6</sub>/CD<sub>3</sub>CN mixtures, the discrete molecular triangle is in equilibrium with the aggregated assembly. This suggests that the solvent composition impacts more likely the equilibrium between both supramolecular forms rather than the size of the multi-scale assembled system. According to TEM experiments the supramolecular particles are isotropic. The control over the shape of the hierarchical self-assemblies remains a very attractive challenge. This could be obtained by controlling additional intermolecular interactions between the primary supramolecular assemblies.<sup>71</sup> Cooperation of different non-covalent interactions, including hydrophobic, electrostatic and hydrogen-bonding ones, is the key to forming ordered extended assemblies with emergent properties.<sup>3,72-74</sup> To this end, the choice of the counter-ions associated to the POM is an important lever in the control of the aggregation process. According to their hydrophilic/hydrophobic character, the counterions should provide segregation<sup>75</sup> in appropriate solvent mixtures and thus allow the control of the nanostructure arrangement as a result of the overall intermolecular interactions at work.

## CONCLUSION

We have synthesized a new ditopic POM-based building-block bearing remote terpyridine units and studied its self-assembly behavior in the presence of a linking metal cation. In a strongly dissociating solvent (DMSO) the hybrid spontaneously assembles into a discrete supramolecular assembly, which was characterized by NMR and SAXS experiments. In the presence of less dissociating solvent (MeCN), the primary supramolecular structure self-assembles into dense monodisperse nanoparticles, characterized through SAXS and HR-TEM, and forms a hierarchical organization, this process being fully reversible. Further studies will focus on the control the shape and size of the overall assembly by modification of the primary POM-based building blocks and their associated counter ions.

## ASSOCIATED CONTENT

### Supporting Information.

The Supporting Information is available free of charge on the ACS Publications website.

Descriptions of the experimental and calculation details.

## ACKNOWLEDGMENT

We acknowledge SOLEIL for provision of synchrotron radiation facilities and we would like to thank Javiez Perez and for assistance in using beamline SWING. We also thank Dr. Sandra Alves for performing the MS analysis of the POM-based building block **D<sub>Si</sub>[tpy]**. The Severo Ochoa Excellence Accreditation (SEV-2013-0319) and the COST Action CM1203 “Polyoxometalate Chemistry for Molecular Nanoscience (PoCheMoN)” are gratefully acknowledged. S.A.S. and C.B. also wish to thank the Marie Curie/COFUND funding scheme (291787-ICIQ-IPMP), the Spanish Ministerio de Economía y Competitividad (MINECO) (CTQ2014-52824-R), the Generalitat de Catalunya (project 2014SGR409), and the ICIQ Foundation.

## AUTHOR INFORMATION

### CORRESPONDING AUTHOR

guillaume.izzet@upmc.fr

### FUNDING SOURCES

No competing financial interests have been declared. This work was supported by the French National Research Agency (EXPAND, ANR-14-CE08-0002). The computational work performed at ICIQ is supported by the Spanish Ministerio de Economía y Competitividad (MINECO) through project CTQ2014-52824-R, by the Generalitat de Catalunya project 2014SGR409, and by the ICIQ Foundation. S.A.S. thanks the Marie Curie/COFUND scheme ref. 291787-ICIQ-IPMP for funding.

## REFERENCES

- (1) Whitesides, G. M.; Kriebel, J. K.; Mayers, B. T. *Self-Assembly and Nanostructured Materials*; Springer: Berlin, 2005.
- (2) Faul, C. F. J. *Acc. Chem. Res.* **2014**, *47*, 3428.
- (3) Rest, C.; Kandanelli, R.; Fernandez, G. *Chem. Soc. Rev.* **2015**, *44*, 2573.
- (4) Chen, L. J.; Ren, Y. Y.; Wu, N. W.; Sun, B.; Ma, J. Q.; Zhang, L.; Tan, H. W.; Liu, M. H.; Li, X. P.; Yang, H. B. *J. Am. Chem. Soc.* **2015**, *137*, 11725.
- (5) Inokuma, Y.; Kawano, M.; Fujita, M. *Nature Chemistry* **2011**, *3*, 349.
- (6) Song, Y. F.; Tsunashima, R. *Chem. Soc. Rev.* **2012**, *41*, 7384.
- (7) Proust, A.; Matt, B.; Villanneau, R.; Guillemot, G.; Gouzerh, P.; Izzet, G. *Chem. Soc. Rev.* **2012**, *41*, 7605.
- (8) Miras, H. N.; Yan, J.; Long, D. L.; Cronin, L. *Chem. Soc. Rev.* **2012**, *41*, 7403.
- (9) Polarz, S.; Landsmann, S.; Klaiber, A. *Angew. Chem., Int. Ed.* **2014**, *53*, 946.
- (10) Yin, P. C.; Li, D.; Liu, T. B. *Chem. Soc. Rev.* **2012**, *41*, 7368.
- (11) Giner-Casares, J. J.; Brezesinski, G.; Mohwald, H.; Landsmann, S.; Polarz, S. *J Phys Chem Lett* **2012**, *3*, 322.
- (12) Noro, S.; Tsunashima, R.; Kamiya, Y.; Uemura, K.; Kita, H.; Cronin, L.; Akutagawa, T.; Nakamura, T. *Angew. Chem., Int. Ed.* **2009**, *48*, 8703.
- (13) Polarz, S.; Smarsly, B.; Antonietti, M. *ChemPhysChem* **2001**, *2*, 457.
- (14) Li, W.; Bu, W. F.; Li, H. L.; Wu, L. X.; Li, M. *Chem. Commun.* **2005**, 3785.
- (15) Scullion, R. A.; Surman, A. J.; Xu, F.; Mathieson, J. S.; Long, D. L.; Haso, F.; Liu, T. B.; Cronin, L. *Angew. Chem., Int. Ed.* **2014**, *53*, 10032.
- (16) Pradeep, C. P.; Misrahi, M. F.; Li, F. Y.; Zhang, J.; Xu, L.; Long, D. L.; Liu, T. B.; Cronin, L. *Angew. Chem., Int. Ed.* **2009**, *48*, 8309.
- (17) Yin, P. C.; Wu, P. F.; Xiao, Z. C.; Li, D.; Bitterlich, E.; Zhang, J.; Cheng, P.; Vezenov, D. V.; Liu, T. B.; Wei, Y. G. *Angew. Chem., Int. Ed.* **2011**, *50*, 2521.
- (18) Landsmann, S.; Wessig, M.; Schmid, M.; Colfen, H.; Polarz, S. *Angew. Chem., Int. Ed.* **2012**, *51*, 5995.
- (19) Jallet, V.; Guillemot, G.; Lai, J.; Bauduin, P.; Nardello-Rataj, V.; Proust, A. *Chem. Commun.* **2014**, *50*, 6610.
- (20) Yan, Y.; Wang, H. B.; Li, B.; Hou, G. F.; Yin, Z. D.; Wu, L. X.; Yam, V. W. W. *Angew. Chem., Int. Ed.* **2010**, *49*, 9233.
- (21) Chakrabarty, R.; Mukherjee, P. S.; Stang, P. J. *Chem. Rev.* **2011**, *111*, 6810.
- (22) Yamada, T.; Otsubo, K.; Makiura, R.; Kitagawa, H. *Chem. Soc. Rev.* **2013**, *42*, 6655.
- (23) He, W. W.; Li, S. L.; Zang, H. Y.; Yang, G. S.; Zhang, S. R.; Su, Z. M.; Lan, Y. Q. *Coord. Chem. Rev.* **2014**, *279*, 141.
- (24) Du, D. Y.; Qin, J. S.; Li, S. L.; Su, Z. M.; Lan, Y. Q. *Chem. Soc. Rev.* **2014**, *43*, 4615.
- (25) Santoni, M. P.; Hanan, G. S.; Hasenknopf, B. *Coord. Chem. Rev.* **2014**, *281*, 64.
- (26) Santoni, M. P.; Pal, A. K.; Hanan, G. S.; Tang, M. C.; Venne, K.; Furtos, A.; Menard-Tremblay, P.; Malveau, C.; Hasenknopf, B. *Chem. Commun.* **2012**, *48*, 200.
- (27) Han, J. W.; Hardcastle, K. I.; Hill, C. L. *Eur. J. Inorg. Chem.* **2006**, 2598.
- (28) Han, J. W.; Hill, C. L. *J. Am. Chem. Soc.* **2007**, *129*, 15094.
- (29) Kang, J.; Xu, B. B.; Peng, Z. H.; Zhu, X. D.; Wei, Y. G.; Powell, D. R. *Angew. Chem., Int. Ed.* **2005**, *44*, 6902.
- (30) Izzet, G.; Macdonell, A.; Rinfrey, C.; Piot, M.; Renaudineau, S.; Derat, E.; Abécassis, B.; Afonso, C.; Proust, A. *Chem. Eur. J.* **2015**, 19010.
- (31) Zhu, Y.; Yin, P. C.; Xiao, F. P.; Li, D.; Bitterlich, E.; Xiao, Z. C.; Zhang, J.; Hao, J.; Liu, T. B.; Wang, Y.; Wei, Y. G. *J. Am. Chem. Soc.* **2013**, *135*, 17155.
- (32) Dong, B.; Sakurai, T.; Honsho, Y.; Seki, S.; Maeda, H. *J. Am. Chem. Soc.* **2013**, *135*, 1284.
- (33) Gröhn, F. *Soft Matter* **2010**, *6*, 4296.
- (34) Willerich, I.; Gröhn, F. *Angew. Chem., Int. Ed.* **2010**, *49*, 8104.
- (35) Klosterman, J. K.; Yamauchi, Y.; Fujita, M. *Chem. Soc. Rev.* **2009**, *38*, 1714.
- (36) Acronyms used for the hybrid POMs: D refers to the Dawson-type anion, Si as subscript relates to the primary functionalization and the term in brackets corresponds to the remote organic moieties.
- (37) Duffort, V.; Thouvenot, R.; Afonso, C.; Izzet, G.; Proust, A. *Chem. Commun.* **2009**, 6062.
- (38) Morris, K. F.; Johnson, C. S. *J. Am. Chem. Soc.* **1993**, *115*, 4291.
- (39) Morris, K. F.; Johnson, C. S. *J. Am. Chem. Soc.* **1992**, *114*, 3139.
- (40) Schaeffer, G.; Fuhr, O.; Fenske, D.; Lehn, J. M. *Chem. Eur. J.* **2014**, *20*, 179.



- (41) Fonseca Guerra, C.; Snijders, J. G.; te Velde, G.; Baerends, E. J. *Theor. Chem. Acc.* **1998**, *99*, 391.
- (42) te Velde, G.; Bickelhaupt, F. M.; Baerends, E. J.; Fonseca Guerra, C.; van Gisbergen, S. J. A.; Snijders, J. G.; Ziegler, T. *J. Comput. Chem.* **2001**, *22*, 931.
- (43) Becke, A. D. *Phys. Rev. A* **1988**, *38*, 3098.
- (44) Perdew, J. P. *Phys. Rev. B* **1986**, *33*, 8822.
- (45) Perdew, J. P. *Phys. Rev. B* **1986**, *34*, 7406.
- (46) Grimme, S.; Antony, J.; Ehrlich, S.; Krieg, H. *J. Chem. Phys.* **2010**, *132*, 154104.
- (47) Grimme, S.; Ehrlich, S.; Goerigk, L. *J. Comput. Chem.* **2011**, *32*, 1456.
- (48) Johnson, E. R.; Becke, A. D. *J. Chem. Phys.* **2006**, *124*, 174104.
- (49) van Lenthe, E.; Baerends, E. J.; Snijders, J. G. *The Journal of Chemical Physics* **1993**, *99*, 4597.
- (50) van Lenthe, E.; Baerends, E. J.; Snijders, J. G. *J. Chem. Phys.* **1994**, *101*, 9783.
- (51) Becke, A. D. *J. Chem. Phys.* **1988**, *88*, 2547.
- (52) Franchini, M.; Philipsen, P. H. T.; Visscher, L. *J. Comput. Chem.* **2013**, *34*, 1819.
- (53) Wang, Y. A.; Yam, C. Y.; Chen, Y. K.; Chen, G. *J. Chem. Phys.* **2011**, *134*, 241103.
- (54) Klamt, A. *J. Phys. Chem.* **1995**, *99*, 2224.
- (55) Klamt, A.; Jonas, V. *J. Chem. Phys.* **1996**, *105*, 9972.
- (56) Klamt, A.; Schürmann, G. *J. Chem. Soc. Perkin Trans. 2* **1993**, 799.
- (57) Klamt, A.; Jonas, V.; Bürger, T.; Lohrenz, J. C. W. *J. Phys. Chem. A* **1998**, *102*, 5074.
- (58) <https://iochem-bd.iciq.es:8443/browse/handle/XXX/YYYY>.
- (59) Vreven, T.; Byun, K. S.; Komáromi, I.; Dapprich, S.; Montgomery, J. A.; Morokuma, K.; Frisch, M. J. *J. Chem. Theory Comput.* **2006**, *2*, 815.
- (60) Frisch, M. J.; Trucks, G. W.; Schlegel, H. B.; Scuseria, G. E.; Robb, M. A.; Cheeseman, J. R.; Scalmani, G.; Barone, V.; Mennucci, B.; Petersson, G. A.; Nakatsuji, H.; Caricato, M.; Li, X.; Hratchian, H. P.; Izmaylov, A. F.; Bloino, J.; Zheng, G.; Sonnenberg, J. L.; Hada, M.; Ehara, M.; Toyota, K.; Fukuda, R.; Hasegawa, J.; Ishida, M.; Nakajima, T.; Honda, Y.; Kitao, O.; Nakai, H.; Vreven, T.; Montgomery Jr., J. A.; Peralta, J. E.; Ogliaro, F.; Bearpark, M. J.; Heyd, J.; Brothers, E. N.; Kudin, K. N.; Staroverov, V. N.; Kobayashi, R.; Normand, J.; Raghavachari, K.; Rendell, A. P.; Burant, J. C.; Iyengar, S. S.; Tomasi, J.; Cossi, M.; Rega, N.; Millam, N. J.; Klene, M.; Knox, J. E.; Cross, J. B.; Bakken, V.; Adamo, C.; Jaramillo, J.; Gomperts, R.; Stratmann, R. E.; Yazyev, O.; Austin, A. J.; Cammi, R.; Pomelli, C.; Ochterski, J. W.; Martin, R. L.; Morokuma, K.; Zakrzewski, V. G.; Voth, G. A.; Salvador, P.; Dannenberg, J. J.; Dapprich, S.; Daniels, A. D.; Farkas, Ö.; Foresman, J. B.; Ortiz, J. V.; Cioslowski, J.; Fox, D. J.; Rev. D.01 ed.; Gaussian, Inc.: Wallingford, CT, USA, 2009.
- (61) Wasielewski, M. R. *Acc. Chem. Res.* **2009**, *42*, 1910.
- (62) Sprafke, J. K.; Kondratuk, D. V.; Wykes, M.; Thompson, A. L.; Hoffmann, M.; Drevinskas, R.; Chen, W. H.; Yong, C. K.; Karnbratt, J.; Bullock, J. E.; Malfois, M.; Wasielewski, M. R.; Albinsson, B.; Herz, L. M.; Zigmantas, D.; Beljonne, D.; Anderson, H. L. *J. Am. Chem. Soc.* **2011**, *133*, 17262.
- (63) Hou, Y.; Zakharov, L. N.; Nyman, M. *J. Am. Chem. Soc.* **2013**, *135*, 16651.
- (64) Yin, P. C.; Zhang, J.; Li, T.; Zuo, X. B.; Hao, J.; Warner, A. M.; Chattopadhyay, S.; Shibata, T.; Wei, Y. G.; Liu, T. B. *J. Am. Chem. Soc.* **2013**, *135*, 4529.
- (65) Wu, Y. L.; Shi, R. F.; Wu, Y. L.; Holcroft, J. M.; Liu, Z. C.; Frasconi, M.; Wasielewski, M. R.; Li, H.; Stoddart, J. F. *J. Am. Chem. Soc.* **2015**, *137*, 4111.
- (66) Svergun, D.; Barberato, C.; Koch, M. H. J. *J. Appl. Crystallogr.* **1995**, *28*, 768.
- (67) Svergun, D. I.; Koch, M. H. J. *Rep Prog Phys* **2003**, *66*, 1735.
- (68) Osborne, E. A.; Jarrett, B. R.; Tu, C. Q.; Louie, A. Y. *J. Am. Chem. Soc.* **2010**, *132*, 5934.
- (69) Als-Nielsen, J.; McMorrow, D. *Elements of modern x-ray physics*; Wiley: New York, 2001.
- (70) Matt, B.; Renaudineau, S.; Chamoreau, L. M.; Afonso, C.; Izzet, G.; Proust, A. *J. Org. Chem.* **2011**, *76*, 3107.
- (71) Whitesides, G. M.; Grzybowski, B. *Science* **2002**, *295*, 2418.
- (72) Luisi, P. *Foundations of Chemistry* **2002**, *4*, 183.
- (73) Hunter, C. A.; Anderson, H. L. *Angew. Chem., Int. Ed.* **2009**, *48*, 7488.
- (74) Bruns, C. J.; Fujita, D.; Hoshino, M.; Sato, S.; Stoddart, J. F.; Fujita, M. *J. Am. Chem. Soc.* **2014**, *136*, 12027.
- (75) Kato, T. *Science* **2002**, *295*, 2414.

SYNOPSIS TOC The metal-driven self-assembly processes of a covalent polyoxometalate (POM)-based hybrid bearing remote binding sites have been investigated. In a strongly dissociating solvent, a discrete metallomacrocyclic is formed while in a less dissociating solvent, the primary supramolecular structure, combining negatively charged POMs and cationic metal linkers, further self-assemble into nanoparticle-like structures.

